CIRP Journal of Manufacturing Science and Technology 38 (2022) 186–203

Contents lists available at ScienceDirect

CIRP Journal of Manufacturing Science and Technology

journal homepage: www.elsevier.com/locate/cirpj

Wire-arc additive manufacturing of structures with overhang: Experimental results depositing material onto fixed substrate

Linn Danielsen Evjemo[a,*], Geir Langelandsvik[b], Signe Moe[c], Morten Høgseth Danielsen[b], Jan Tommy Gravdahl[a]

[a] Norwegian University of Science and Technology, O. S. Bragstads plass 2D, Gløshaugen, Trondheim, Norway
[b] Department of Materials and Nanotechnology, SINTEF Industry, Trondheim, Norway
[c] SINTEF Digital/Sopra Steria, Oslo, Norway

ARTICLE INFO

Available online 13 May 2022

Keywords:
Additive manufacturing
Wire arc additive manufacturing
Cold metal transfer
Arc Welding
Robotics

ABSTRACT

As additive manufacturing (AM) technology grows both more advanced and more available, the challenges and limitations are also made more evident. Most existing solutions for AM build structures layer by layer using strictly vertical material deposition. As each layer must vertically adhere to the previous layer, support structures must be added if there are to be any kinds of overhangs. For methods requiring the build to be performed within a chamber, the size of the structure is also very limited. The research presented in this paper explores possible solutions to these challenges, focusing on wire-arc additive manufacturing in order to effectively build structures that can not easily be constructed using in-box, layer-based methods for AM. By non-vertical material deposition using an industrial robot manipulator, metal structures with overhangs are built onto a fixed, horizontal surface without any support structures. Cross sections of two different structures are examined by optical microscopy and hardness measurements to reveal potential differences between the areas with and without intersections or overhang.

Introduction

Over the last decades, additive manufacturing (AM) has become increasingly important for low-cost prototyping and customisation. AM is the umbrella term that covers many different techniques for building up a 3D structure, such as 3D-printing, rapid prototyping (RP) and free-form fabrication [1]. Out of these, 3D printing is perhaps the most available method, as desktop 3D-printers have become both affordable and easier to use for both professionals and enthusiasts. Even if AM technology has made prototyping and modelling easier, there are still some major limitations for most traditional methods of AM. Depending on the AM method, the challenges can vary from issues such as long build time or high cost [2] to issues related to structural challenges such as residual stresses or porosity within the final structure [3]. This research aims to address how to get around two of the most pronounced challenges: limitations on geometrical design and size.

Many widely used methods for AM require the AM process to be done 'in-box', such as powder bed fusion (PBF) or vat polymerisation (VP). In other words, the build must be conducted inside a chamber filled with powder or liquid material that is hardened layer by layer, gradually building up the structure [1]. Other methods use localised material feeding in some form, such as powder based direct energy deposition (DED) or material jetting (MJT), but are still limited by the size of the AM apparatus because the material extrusion happens strictly vertically in a 3 DOF gantry-like machine. This means that for AM techniques that require a build chamber or a basin, the AM machine must be larger than the structure being constructed, which greatly limits the build volume. This is generally not the case with some methods for DED such as AM done by arc welding, where material deposition is made without the limitations of an enclosed space. In addition, some projects have over the last years scaled up extrusion based AM systems in order to build full-size houses [4,5]. These set-ups prove useful in construction, but they are tailored for this purpose, and deposit material faster and with lower accuracy compared to smaller 3D printers. They are therefore not suited for producing metal parts at a low scale, etc.

Even though commercial 3D-printers more suited for building prototypes or end-products are growing in scale, a large 3D-printer is still in most cases limited to a chamber of less than one-by-one

* Corresponding author.
E-mail addresses: linn.d.evjemo@ntnu.no (L.D. Evjemo), geir.langelandsvik@sintef.no (G. Langelandsvik), signe.moe@soprasteria.com (S. Moe), morten.danielsen@sintef.no (M.H. Danielsen), jan.tommy.gravdahl@ntnu.no (J.T. Gravdahl).

https://doi.org/10.1016/j.cirpj.2022.04.006
1755-5817/

metre. This is why AM has mostly been used for creating relatively small end products, or smaller parts for larger products. With AM by material deposition, there is no excess material that needs to be contained, so it is not necessary to do the build in-box. If material deposition can be combined with for example an industrial robot manipulator, the work-space will increase dramatically. Attaching the robot manipulator to an actuator rail can increase the work-space even further.

AM methods based on vertical material deposition and a layer-by-layer building process are also somewhat limited with respects to the obtainable geometry of the structure. Most AM methods execute the build strictly layer by layer, either bottom-up or top-down, and the material is deposited or set using a tool which is limited to Cartesian movements. Though many path planning strategies exist, layers are generally applied directly on top of each other, as all material must be vertically attached to the previous layer [6]. Building any kind of overhang may therefore require additional support structures to be included in the build, which means more materials and a longer build time [7]. If the cavities or overhangs are significant for the final product, the support structures must be removed in post-processing. Different AM technologies demand different kinds of support structures with their own advantages and disadvantages, and minimising side effects such as extended build time or additional material cost is important as AM technology becomes more commonly used in industry [7]. Some AM methods with a relatively low building rate due to thin layer heights, such as PBF or VP, allow for overhangs because the otherwise unsupported parts of the structure can rest on underlying excess material, such as a powder bed. Still, if overhangs could be built without the need for such support structures or other kinds of additional support for methods with a higher material deposition rate, such as DED or material extrusion, this could save both time and materials.

A 6 degrees-of-freedom (DOF) robot manipulator can move its end effector with an attached tool to any point within its workspace and with an arbitrary orientation. If fast-curing material was deposited using such a 6 DOF robot arm, material could be deposited non-vertically, removing the need for support structures. The building material would still have to be attached to previously deposited material, but if this could be done at an angle, support structures might be superfluous.

The research presented here will focus on depositing material onto a *fixed* surface using a 6 DOF robot arm. Similar work have been done on AM processes with a *moving* building surface about a fixed point of material deposition, both using plastics [8] and metals [9,10]. The aim of the research presented in this paper is to see how feasible the former approach is. Though an approach with a fixed point of material deposition shows promise, a mobile point of material deposition could make AM more applicable to a factory setting, repair work on-site etc., as it is more flexible. Joris Laarman Lab has done some work using this approach, with very promising results. They have used both stainless steel [11] and a fast-curing polymer [12] in their builds, but none of their algorithms or control methods have been made public.

AM methods such as VP or powder based DED often build with a high accuracy and resolution, and would consequentially be quite time-consuming for larger components, depending on the application. The build time of a component is generally decided by the part size, layer thickness, printing speed and build orientation: When high accuracy is necessary, the layers are often very thin. As building in the z-direction is then quite time consuming, time could be saved by orienting the structure so that the build height is kept at a minimum [2]. However, for structures that will in any case need some post-processing or machining, the resolution and layer height can be reduced in order to make the build more efficient. This could for example be the case when working with AM in metal, or more specifically wire-arc additive manufacturing (WAAM), which also falls under DED type AM methods [13,14].

This paper presents how it was possible to build structures with overhang on a horizontal surface with no need for additional support structures, and with continuous material deposition. Using welding equipment attached to a 6 DOF robot manipulator, material could be deposited using a non-vertical orientation of the welding tool. In addition, the constraints on the size of the build was greatly reduced compared to many in-box methods, as the size of the structure was only limited by the workspace of the robot. Preliminary results were presented in [15–17], and in this paper these results will be extended by experiments building structures with overhangs. Experiments with overhang were performed both with a fixed and an adjustable orientation of the tool.

In *Preliminary tests with viscous material* some preliminary experiments for a none-layer wise build using viscous glue and set-based control, are presented. *Working with metals: WAAM and CMT* explains the shift to building in metals, and the principles behind WAAM and the arc welding method cold metal transfer (CMT). *Continuous build of thin-walled structures* explores building thin-walled structured continuously using WAAM, as continuous material deposition is desirable to keep the building time low. If the structure is more complex, some challenges related to intersections and corners may arise, and this is the focus of *Avoiding double material deposition in intersections*. *Set-based control for flexibility in orientation of tool* presents how the set-based method used for the preliminary experiments from *Preliminary tests with viscous material* was also used on metal structures. Finally, *Structures with overhang focuses* on structures with overhangs, and how the workspace and flexibility of a 6 DOF robot manipulator makes it possible to deposit material with a non-vertical orientation of the tool onto a fixed substrate. Material analyses of one of the structures with intersections in addition to one of the structures with overhangs are presented in *Material analysis*, considering the differences in parts of the structures with and without intersections or overhangs.

Preliminary tests with viscous material

In order to outline the direction of this work, a review of the current status of large-scale AM was conducted, presented in [15]. A small-scale proof-of-concept experiment was designed to map how a viscous material with dynamic viscosity of 3.200.000 mpa s at 25 °C [18] could be used to build a cylindrical cup-structure in a continuous, non-layer-wise movement. The height increase was continuous, taking a step away from the strictly layer-wise approach in traditional AM methods. Several tests were carried out using a air-pressure driven caulking gun attached to a 6 DOF UR-5 robot manipulator. Using the print head of a 3D printer attached to the robot's end effector was considered, but discarded as it was preferable to deposit material more quickly (Fig. 1).

One of the resulting structures from the caulking gun experiments is shown in Fig. 2. These tests indicated that AM by robot manipulator was possible, and illustrated some of the main challenges related to continuous material deposition that had to be addressed in later work. Starting and stopping the flow of material proved especially challenging, and greatly factors into why the aim is continuous material deposition. The control method used in these experiments were later used to test how a non-vertical orientation of the tool impacts the build in a WAAM process, presented in *Set-based control for flexibility in orientation of tool*. More details regarding the control methods and approach from the preliminary experiments, as well as the state-of-the-art review, can be found in [15]. Full details on the set-based control method can be found in [19,20].

Fig. 1. Robot cell used in preliminary experiments presented in Preliminary tests with viscous material: 6 DOF UR-5 robot manipulator with air-pressure driven caulking gun.

Working with metals: WAAM and CMT

Building structures in metal using AM could be useful in many different industries. Post-processing of structures in metal is often required, even for relatively quick procedures such as metal casting. This reduces the necessary resolution of the build, which makes it more feasible to get the production time down compared to traditional AM methods. AM in metals could be applied in repair work, for example on ships or other structures that would benefit from having repairs done on-site, as well as in building custom-designed metallic parts or end-products.

Fig. 2. Cylindrical cup-structure built in preliminary experiments described in *Preliminary tests with viscous material*. Approx. 4 cm tall, built using a viscous glue.

The work presented here will focus on WAAM, a method where welding equipment is generally attached to the end effector of an industrial robot manipulator. Gas metal arc welding (GMAW), often referred to as metal inert gas welding (MIG), is preferred as a method for robotised WAAM as it is generally easier to implement. While for example gas tungsten arc welding (GTAW), also known as tungsten inert gas welding (TIG), has external feeding of the welding material, the welding material in MIG is fed through the nozzle of the welding gun, thereby acting as the electrode [21]. This means that there is only the nozzle of the welding gun to consider when designing the path for the robot's end effector, as opposed to the additional external obstacle that the wire feed in a TIG process would introduce.

The modified metal inert gas welding method cold metal transfer (CMT) has a more stable arc than traditional GMAW, which reduces metal spattering or 'welding sparks'. It also has a reduced heat input, which reduces residual stresses and distortions [22]. These properties make CMT well suited for WAAM, and the objective was consequently to focus on CMT in this research. A series of different experiments were done in collaboration with SINTEF Industry using a 6 DOF IRB 2400/10 robot manipulator from ABB robotics [23], shown in Fig. 3, equiped with Fronius TPS 400i CMT welding equipment [24]. For some of the experiments, the heat-input provided by CMT was not sufficient for the deposited material to properly adhere to the substrate. For these instances, pulsed-MIG welding was used for either the first few layers or the entire build. Pulsed-MIG is a modified GMAW welding method with a higher heat input than for CMT, but where the current alternates between a high and a low current level [25]. This makes it possible to transfer material with a lower heat input than for standard spray arc GMAW welding, as the melt bath does not have time to solidify between pulses, and the welding method is less vulnerable to spatter [21].

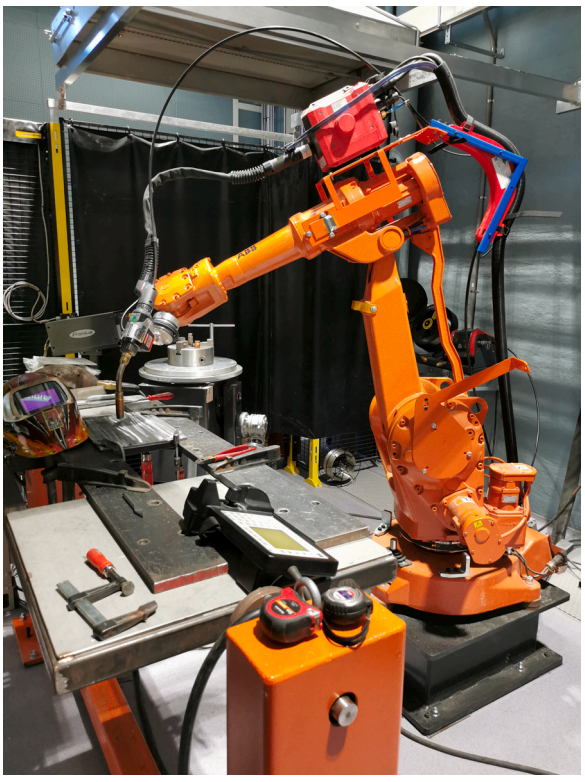

Fig. 3. Lab set-up: Robot cell used in WAAM experiments. 6 DOF ABB IRB2400 robot manipulator with CMT welding equipment from Fronius. This set-up was used in all the experiments presented here.

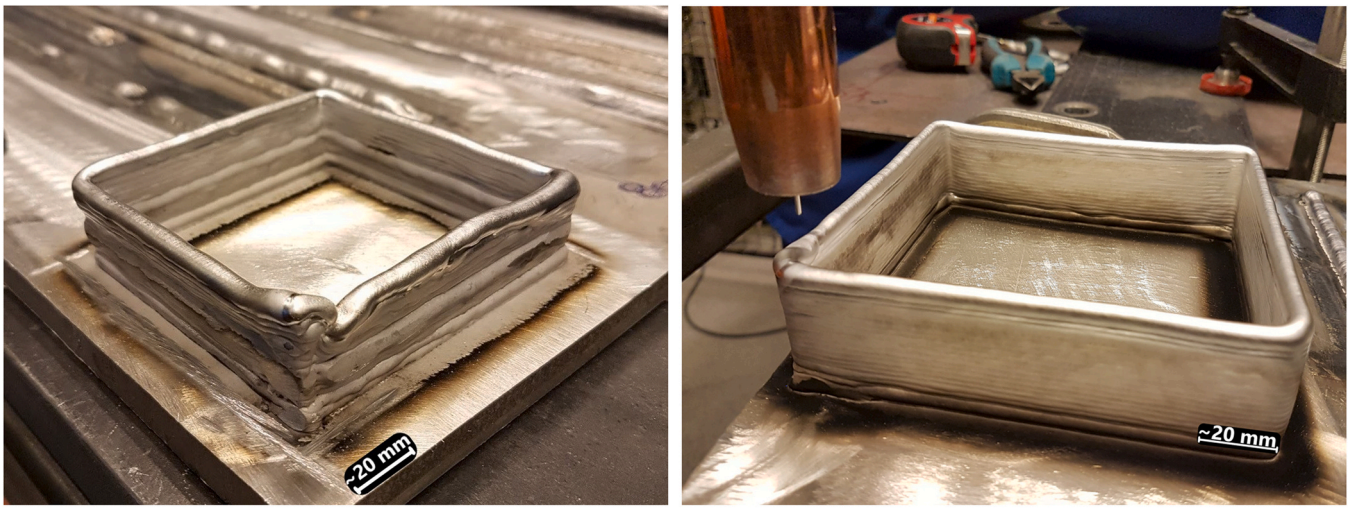

(a) First CMT box build with clear visual flaws due to accumulated errors.

(b) Second, modified CMT box build with smoother walls and few distortions.

Fig. 4. Square-box: Adjusting the structure to have smoother layer transitions, blunter corners and longer sides clearly improved the visual appearance of the structure.

Continuous build of thin-walled structures

Though WAAM in many ways differs greatly from deposition of glue through a caulking gun, the challenges related to beginning and ending the material deposition are quite similar. Just as the variations in the material flow created imprecisions in the viscous glue build, arc initiation and flame-out will generally create irregularities due to uneven material deposition for WAAM [26]. Achieving a building process that is as continuous as possible can help remove some of the challenges related to starting and stopping the material deposition revealed through the preliminary experiments [15]. A continuous building process can also make the build less time-consuming, which in an industrial setting is important in order to make production cost-effective.

In order to investigate how the heat development of prolonged deposition would impact the structure on a superficial level, the first tests focused on constructing a square, thin-walled box by continuous material deposition and CMT welding. The building material was aluminium, and the alloys AA4043 and AA4047 were used. For details related to the welding parameters, see [16].

The robot path was programmed using linear arc welding functions in the programming language Rapid, developed by ABB. Unlike the structure build in the preliminary glue experiments, this square structure did not have a continuous height increase, but was constructed in a semi-layer-wise manner. The height increase necessary to begin building the next layer was carried out evenly over the last few centimetres of each layer, which resulted in a smooth build with no visible irregularities. The difference between increasing the height of the welding gun in a *single point* vs. over a few centimetres can be seen in Fig. 4. Seemingly, increasing the height in a single point lead to a heap-up of material, while a gradual height increase resulted in a smooth transition between layers. This method was kept for further experiments with a semi-layer-wise design, and later adjusted to a completely continuous movement in the z-direction. However, for simple structures the difference between a fully continuous height increase and an increase over a few centimetres for each layer seemed negligible.

The results of the two first tests are shown in Fig. 4. The experience from these tests made it possible to later build much taller, similar structures with continuous material deposition. Some of these are shown in Fig. 5 and Fig. 19. Heat accumulation did not seem to impact the shape of the structures in any significant way, so these builds could have gone on for much longer without any difficulty. The latter is built using the Ni-Cr-Mo alloy UTP 759 instead of an aluminium alloy, which seemed to make the heat accumulation quite insignificant even for a more complex structure, see *Avoiding double material deposition in intersections*.

Avoiding double material deposition in intersections

The box builds presented in *Continuous build of thin-walled structures* are relatively simple geometrical structures. For more complex shapes built in a semi-layer-wise manner, issues related to intersections might appear. When deposing material continuously, which is desired for efficiency, intersections within the same layer will potentially lead to double deposition of material in the point of the intersection. Starting and stopping the welding process before and after crossing a welding bead is not considered to be a good solution, as arc initiation and arc flame-out leads to uneven material deposition [26].

One solution to this challenge was examined: avoiding actual intersections by designing non-crossing paths within each layer, as

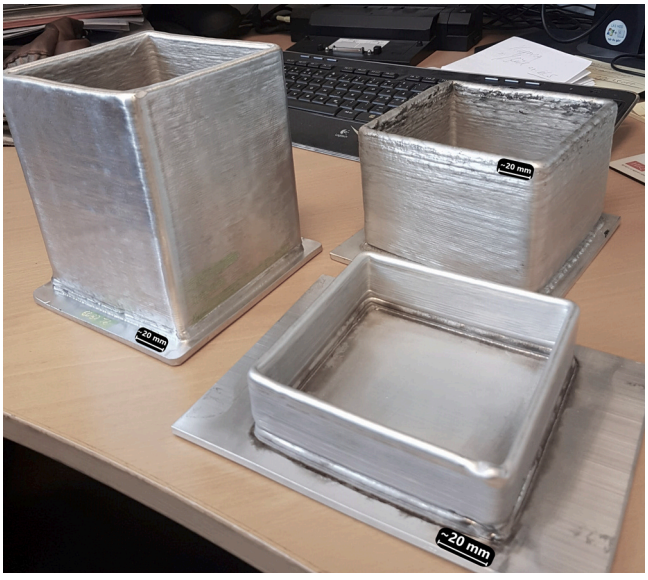

Fig. 5. Taller builds: After initial tests with square structures in aluminium, it was possible to build guide tall structures using material deposition.

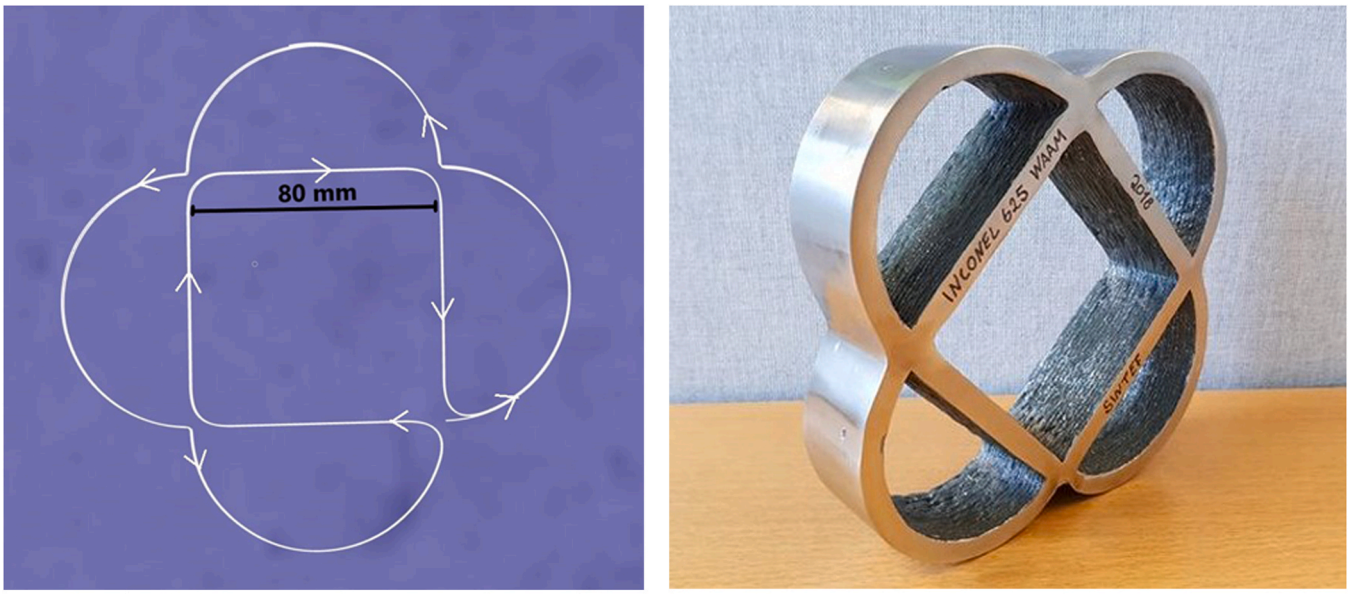

(a) First CMT box build with clear visual flaws due to accumulated errors.

(b) Second, modified CMT box build with smoother walls and few distortions.

Fig. 6. Path design: Intersections are avoided altogether by instead designing a path consisting of closely placed opposite corners. After post processing on the Inconel 625 structure shown in Fig. 7, it was evident that the structure had welded together adequately. (a) and (b) have the same scale.

shown in Fig. 6. This method, where intersections are created by opposing corners, is described in [27]. Experiments were done using this method to build what will from here-on be described as flower structures, as shown in Fig. 6 and 7. The building material was aluminium AA4043 and AA4047, as well as the nickel-based alloy Inconel 625 and the Ni-Cr-Mo alloy UTP 759. Building in different materials helped assess the effect of the physical properties of the welding material, as the aluminium alloys had a much lower melting point than the nickel alloys. The aluminium builds were done using CMT and pulsed-MIG welding. The builds in nickel-based alloys were done using only pulsed-MIG, as this material requires a higher heat input that available when using CMT.

The non-crossing paths strategy used in these tests seemed to work well when building with relatively hard materials with a higher melting point, such as Inconel 625. When building with aluminium, the inner walls of the flower structure began to slope. The heat dissipation was hampered by the surrounding walls, closing the heat in, and leaving the deposited material liquid for a longer time period. The material would therefor spread out over a larger area before solidifying, resulting in considerable differences in the height of the deposited welding bead within each layer. In addition, the intersections became points of heat accumulation, with even more severe contortions. The inaccuracies caused by the uneven cooling and deposition of material would accumulate over time, introducing a need to periodically pause the continuous process to manually grind the structure down to an even height. It was possible to improve the aluminium structures by tuning the heat input and other welding parameters, as shown in Fig. 7. However, it was much easier to build this structure using a metal with a higher melting point, because this material would solidify faster, and thereby make the structure less vulnerable to contortions caused by accumulated heat as the build progressed. The structure built in Inconel 625 was cut from the base plate and polished, and after post processing it was possible to determine that the path had in fact welded together adequately in the intersection points, as shown in Fig. 6. Further details on this experiment can be found [16].

Set-based control for flexibility in orientation of tool

One of the main advantages of depositing material using a 6 DOF robot arm is the ability to orient the tool so that material can be deposited in any direction, not just strictly vertically. Therefore, the next step after building simple, thin-walled structures using continuous material deposition was to vary the orientation of the tool. An overhang is a part of the structure that sticks out over a lower part of the structure without being supported by an preceding layer in a directly vertical direction. AM using non-vertical material deposition makes it possible to build structures with overhangs without additional support structures, and geometries that might not be available when using methods such as PBF or VP.

The method for set-based control used in the preliminary experiments in *Preliminary tests with viscous material* can also be applied to WAAM with a non-vertical deposition of material. This framework works well for robotic systems with a large number of DOFs and several tasks to solve. It combines set-based tasks defined by a valid interval, for example collision avoidance, with equality tasks defined by a desired value, such as position control for the end effector [19]. While the desired behaviour of the robot can often be described in such a task space, the robot control is actually done in the joint space, i.e. feeding the controller a specific set of desired joint values. Set-based control is a kinematic control framework which calculates reference states based on the desired behaviour and the current state of the system. For a detailed description of this framework, please refer to [19,20].

For experiments with material deposition by robot manipulator, there are two tasks that need to be handled: Position control to make sure the end effector follow the desired welding trajectory, and orientation control of the end effector. Position control can be defined with an equality task that must be met at all times. This ensures that the position of the nozzle is accurate and predictable, which is increasingly important when deposition material in a relatively narrow bead. If more material is deposited at a time, resulting in a wider building surface, the position of the tool can

(a) Aluminium AA4047.

(b) Nickel-based alloy Inconel 625.

(c) Aluminium AA4043.

(d) Ni-Cr-Mo alloy UTP 759.

Fig. 7. Varying results: The resulting thin-walled structures based on the pattern in Fig. 6, built using four different welding materials. The scale of these structures matches that of the sketch in Fig. 6a, i.e. the sides of the inner square are 80 mm long.

potentially be allowed to deviate more than the guaranteed position control accuracy of under 1 mm for the IRB2400/10 [23]. For the preliminary experiments presented in *Preliminary tests with viscous material*, the orientation control can also be considered an equality task, as the tool has to stay perpendicular to the welding surface. However, changing the control of the orientation of the tool to instead be considered a set-based task can add freedom in the orientation of the tool. This allows the orientation of the tool to deviate with a few degrees from a set orientation, while keeping control of how large such a deviation can become by adjusting the size of the valid set. Such an approach shows promise in other applications such as spray painting [20].

Using set-based control method that give us some deviation in the orientation of the tool will make the movements smoother and less demanding for the robot compared to a strictly vertical orientation, as one less constraint has to be considered while the orientation stays within the defined set. Keeping a constant speed for the movement of the tool, especially at a relatively high speed, is demanding for the robotic system due to the large torques that are needed. The set-based method designed by Moe et al. may reduce the required torques, as the freedom in orientation helps enable a smoother trajectory for the tool [20]. This also expands the robot's work-space, and can allow for movements that would not be feasible using a constant orientation of the welding gun.

The WAAM experiment using the set-based control framework was designed to build a structure with the same kind of path as for the initial experiments using glue [15], which resulted in the structure in Fig. 2. The orientation control was designed so that the orientation of the tool had to stay within the interval of a few degrees defined by the set-based task, e.g. 10°. As long as this set-based task was met, the motion was controlled only by the equality task defining the path. A bottom layer was built in an outwards spiralling path, as shown in Fig. 8, which then continued on in a helix-path with steady height increase.

It was desired to build these structures using CMT welding, as this had worked well for the simple geometrical shapes described in *Continuous build of thin-walled structures*. Using CMT had resulted in smooth surfaces and builds that seemed to could continue for a long time without excessive heat build-up and bead overflow [16]. However, the base plates available for use in the set-based experiments were thicker than those using in previous experiments. This required a higher heat input in order for the first few welding beads to adhere sufficiently to the substrate. As this helix structure also included a bottom layer, the heat input had to be high enough for the

Fig. 8. Set-based: The structure was a cylindrical shape. The bottom layer was constructed in a outwards spiral, while the path for the wall was an upwards helix with a constant radius and a constant height increase.

spiral to melt together to create a smooth surface. Therefore, the spiralling bottom layer was built using pulsed-MIG, while CMT, with a lower heat input, was used for the rest of the build.

Structures with overhang

One of the main motivations for depositing material with a 6 DOF robot manipulator is to be able to build structures with overhangs. Due to strictly vertical deposition of material, overhangs can traditionally not be build using extrusion based AM methods without adding support structures that must be removed in post-processing. Depositing material non-vertically can remove the need for support structures, which simplifies the building process, and helps save time and materials. It can also allow for a non-layer-wise approach to the AM process, as demonstrated by Laarman Lab and their artistic builds done in a fast-curing polymer [12,15].

Two different methods for creating overhangs were examined: First, testing how overhangs can be “forced" by depositing material vertically onto a lower part of the structure which only partially overlaps with the current path. Material analyses were performed to examine the quality of two the final structures, i. e. optical microscopy and hardness measurements. This will be examined further in *Material analysis*. Then, two different structures with more prominent overhangs were constructed by modifying the orientation of the tool’s nozzle to follow the incline of the overhang (Fig. 9).

Fixed orientation of tool: Twisting hexagon

Using the same robot cell as for the former welding experiments (ABB IRB2400/10 6DOF robot manipulator and Fronius TPS 400i GMAW welding equipment with CMT) a thin-walled structure similar to those described in *Continuous build of thin-walled structures* was constructed. The geometric shape making out the foundation for the build was changed to a regular hexagon instead of a square. The linear movement functions in the Rapid programming language were used to build the structure, which made it necessary to define the path using Cartesian coordinates relative to a start point p_c. A regular hexagon as shown in Fig. 10 has 6 equal angles and six equal sides, and the distance from the centre point p_c to each vertex equals the radius r of the circumscribed circle. The apothem, i.e. the shortest distance l from the centre point p_c to each side, equals the radius of the inscribed circle, and $l = \frac{\sqrt{3}}{2}r$ [28]. The points describing the position of the six vertices in Fig. 10, relative to the Cartesian centre point $p_c = [x, y, z]$ of the hexagon were found using these geometrical relations:

$$p_1 = p_c + [-r, 0, 0] \tag{1}$$

$$p_2 = p_c + \left[-\frac{1}{2}r, \frac{\sqrt{3}}{2}r, 0\right] \tag{2}$$

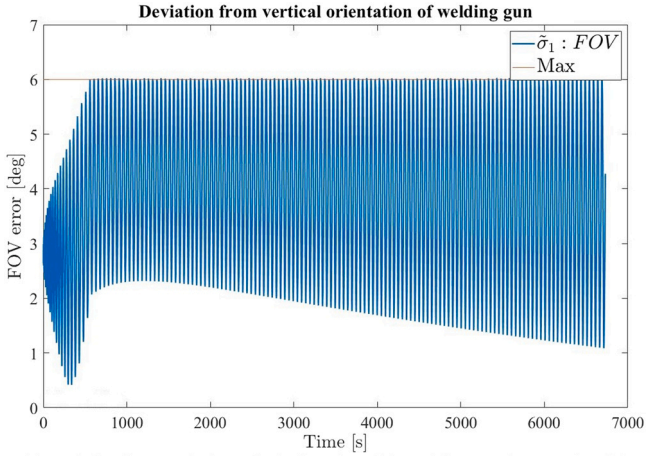

(a) Deviation from a strictly vertical orientation of the welding gun, between 1 and 6 degrees.

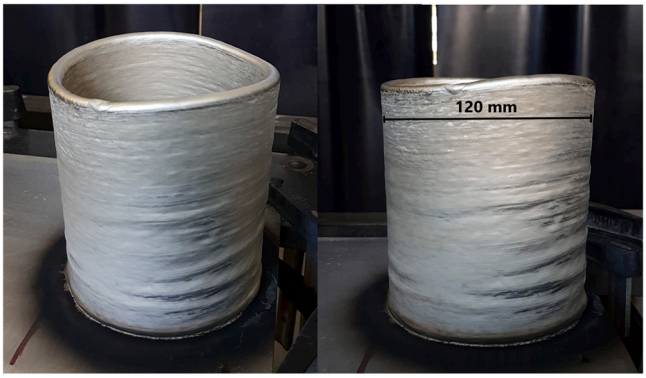

(b) Final structure built using set-based control.

Fig. 9. Build using set-based control, with deviation for vertical orientation of welding too.

$$p_3 = p_c + \left[\frac{1}{2}r, \frac{\sqrt{3}}{2}r, 0\right] \tag{3}$$

$$p_4 = p_c + [r, 0, 0] \tag{4}$$

$$p_5 = p_c + \left[\frac{1}{2}r, -\frac{\sqrt{3}}{2}r, 0\right] \tag{5}$$

$$p_6 = p_c + \left[-\frac{1}{2}r, -\frac{\sqrt{3}}{2}r, 0\right] \tag{6}$$

The base layer was approx. 14 cm wide, as the length r in Fig. 10 was set to be 7 cm. In order to generate an overhang, this hexagonal shape was rotated slightly for each layer. The orientation of the welding gun was fixed, keeping it orthogonal on the base plate. The height increase between layers were spread out over the sixth side of the hexagon, between point p_6 and p_1. For each layer, the hexagon was rotated with an angle $\theta = 1.2^\circ$ about the centre, leading the structure to twist as the build grew taller.

How this creates an overhang can be understood studying Fig. 10: The distance r from the centre of the hexagon to the vertex p_5 corresponds to the hypotenuse of a right-angled triangle. As vertex p_5 rotates about the centre with an angle θ, this distance remains the same. As the hypotenuse of a right-angled triangle is longer than its legs, the vertex p_5 will end up outside the side p_5p_6 of the first layer. With no support structures added, this creates a small overhang as the build continues.

The structure was built using CMT welding, except from the first two layers: As for the structure described in *Set-based control for flexibility in orientation of tool*, these had do be welded using pulsed-MIG for

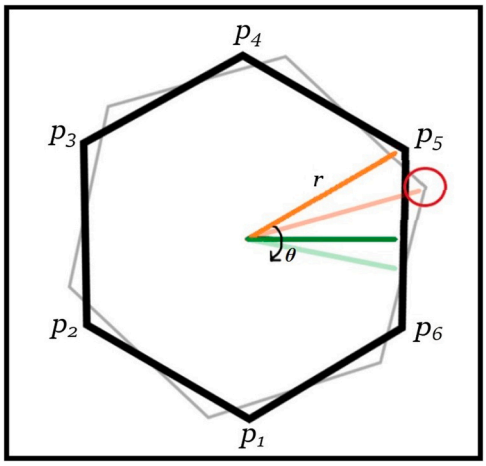

Fig. 10. Hexagon: As corner A rotates with an angle θ about the centre in an arc with radius r, it creates an overhang, as marked with a red circle.

the heat-input to be high enough for the deposited metal to adhere sufficiently to the substrate. The welding wire was made of the Ni-Cr-Mo alloy UTP 759, and the substrate was made of carbon steel S355G10. The parameters for the welding process are listed in Table 1. This build went on for approx. 45 layers, which meant that each corner of the hexagon had rotated about 53° away from its starting point.

As the aim of this experiment was to study the overhang, a rotation close to 60° was enough, as vertex p_5 in Fig. 10 at this point of the build would have rotated all the way to overlap with vertex p_6. After only 25 layers each of the vertices would have rotated 30°, and be at the point where the overhang was largest relative to the first layer. When studying Fig. 10, the orange line r for the current layer would then overlap with the original green line making out the longest leg of a right-angled triangle with hypotenuse r. The size of the overhang would be equal to the difference between r and l, which meant that the overhang protruded

$$r - l = r - \frac{\sqrt{3}}{2}r = 70 - \frac{\sqrt{3}}{2}\cdot 70 = 9.38$$

millimetres over the base layer of the structure. As the welding bead was approx. 4 mm wide, this equals more than twice the width of the welding bead (Fig. 11).

Non-vertical material deposition: Vase

Next, a structure with a significant structure was constructed by depositing material non-vertically. This design was a variation of the cylindrical structures from the experiments presented in *Preliminary tests with viscous material* and *Set-based control for flexibility in orientation of tool*. The difference is to have a varying radius, which in

Table 1
Welding parameters for twisting hexagon structure: Fixed orientation of tool mainly using CMT welding.

Hexagonal structure shown in Fig. 11						
CMT, fixed orientation of tool						
Method	Layer	Current (A)	Wire-feed speed (m/min)	Voltage (V)	Bead height (mm)	Rotation (degrees)
P-MIG	≈ **1**	182	7.1	25.5	1.5	0.0
P-MIG	≈ **2**	154	7.1	25.1	1.5	1.2
CMT	≈ **3**	130	3.8	20.9	1.5	2.4
CMT	≈ **4**	108	3.8	15.4	1.5	3.6
CMT	≈ **5–44**	95	3.8	15.9	1.5	4.8 + =1.2
CMT	≈ **45**	95	3.8	15.9	1.5	52.8

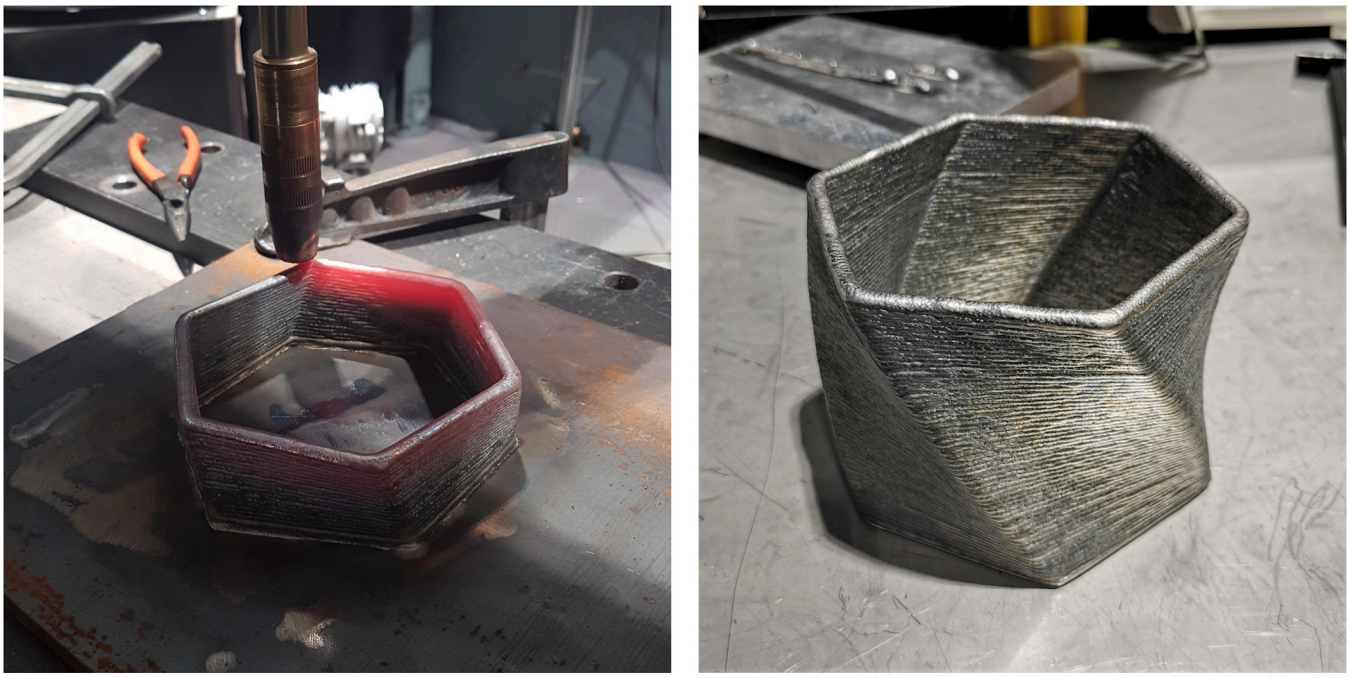

(a) The structure glowed red hot during construction. (b) The final hexagon shape, approx. 45 layers tall.

Fig. 11. Using a fixed vertical orientation of the welding gun, it was possible to construct a structure with a slight overhang. Spiralling hexagon, built in UTP 759.

turn creates an outwards or inwards overhang. A simulation of this path is shown in Fig. 12, and the design will from here-on be referred to as a vase shape.

As explained in *Set-based control for flexibility in orientation of tool*, the set-based method described in [19,20] prioritises the ease of the robot movements in order to create a smooth trajectory. However, the deviation in the orientation of the tool is not necessarily distributed symmetrically. For a traditional cylindrical shape, this imbalance in the change in the orientation resulted in the tool being almost vertical on the part of the build closest to the robot manipulator, and tilted slightly outwards on the opposite side. This in turn resulted in a saddle form at the top of the constructed cylinder, as shown in Fig. 9 [16]. The method was still tested on the vase shape in order to see how this would impact a structure with overhang. The build was done using UTP759, the same Ni-Cr-Mo alloy used for the hexagonal structure in Fig. 11.

The experiment using set-based control to build a vase structure was terminated after just a few layers. The non-symmetrical change in the orientation of the tool followed the pattern of the cylinder structure from Fig. 9, with the welding gun being almost vertical on one side of the build. This showed the significance of the orientation of the welding gun: On the side where the tool remained almost vertical, the deposited material did not adhere evenly with the previous layer, as the overlap with the previous layer was not large enough. This resulted in cladding of material, which only grew worse from one layer to the next. Welding parameters etc. for this interrupted experiment were not included in this paper, as a close analysis of this test was deemed not relevant.

However, on the opposite side of the structure, the orientation of the tool was almost aligned with the tilt of the overhang, as the welding gun tilted outwards while the radius of the structure was increasing. On this side, the constructed wall was smooth and without obvious deformation. This indicated that building such a structure while forcing the orientation of the welding gun to match the angle of the tilt of the wall would likely be more successful.

For the ensuing experiment, the path was programmed directly using the linear functions in the RAPID programming language [29], with set values for the orientation of the welding gun. The orientation of the welding gun was adjusted to being close to parallel with the direction of the tilt of the wall creating the overhang. This can be better understood by studying Fig. 12, which shows a simulation of the welding process performed in ABB's simulation software Robot Studio: As long as the radius is increasing, the welding gun will be oriented slightly outwards, and vice-versa. As the nozzle is symmetrical, no rotations about the global z-axis are needed, i.e. the axis perpendicular to the substrate, pointing out of the page when studying Fig. 13. The structure is designed to first have a section with an increasing radius, then a section with a constant radius, and lastly a section with a decreasing radius. The shift in orientation is introduced gradually over a few layers in between these sections, as listed in table 2.

The RAPID functions used to control the robot during these experiments requires the desired orientation of the end effector to be presented in quaternions $\boldsymbol{q}$, defined as [30]:

$$\boldsymbol{q} = q_\omega + \boldsymbol{i}q_x + \boldsymbol{j}q_y + \boldsymbol{k}q_z \tag{7}$$

In order to control the rotation of the tool relative to the world frame, which is parallel with the build, rotation matrices are used. Given a set of quaternions, the corresponding rotation matrix $\boldsymbol{R}_0$ can be derived. The desired rotations about the world x- and y-axes can then be performed on this rotation matrix, which will result in a new rotation matrix $\boldsymbol{R_N}$ corresponding with the final orientation of the end effector. The corresponding quaternions for the new orientation, $\boldsymbol{q_N}$, can be found from the rotation matrix $\boldsymbol{R_N}$, and used as input for the built-in RAPID functions that control the robot arm [29].

When reading the quaternions $\boldsymbol{q}$ representing the orientation of the tool when placed in a vertical position, the rotation matrix $\boldsymbol{R_0}$ for the orientation of the tool was found using the following equation [31]:

$$\boldsymbol{R}_0 = \begin{bmatrix} 1-2q_y^2-2q_z^2 & 2q_xq_y-2q_zq_\omega & 2q_xq_z+2q_yq_\omega \\ 2q_x2_y+2q_zq_\omega & 1-2q_x^2-2q_z^2 & 2q_yq_z-2q_xq_\omega \\ 2q_xq_z-2q_yq_\omega & 2q_yq_z+2q_xq_\omega & 1-2q_x^2-2q_y^2 \end{bmatrix} \tag{8}$$

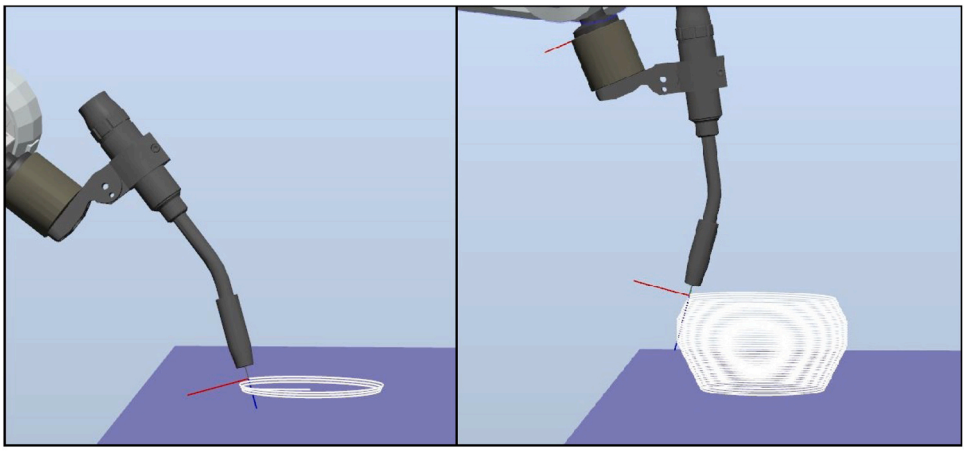

(a) The tool was oriented semi-parallel to the direction of the overhang being constructed.

(b) Vase structure, built in UTP 759.

(c) Profile of the vase.

Fig. 12. Building more prominent overhangs proved successful when orienting the tool relative to the building direction.

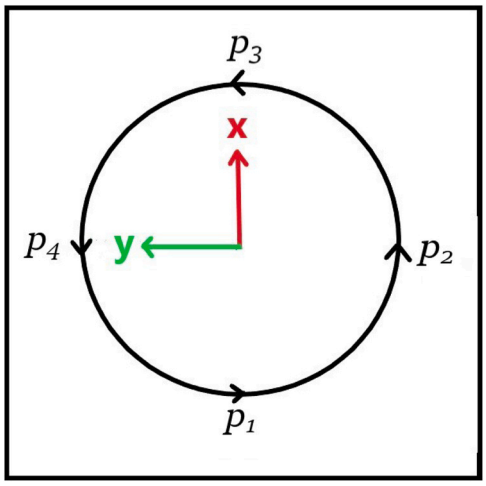

Fig. 13. Base with axes: This circle is the base for the vase structure in Fig. 12, and the axes show the global x- and y-axes that the welding gun is oriented relative to.

As can be seen from Fig. 12, the tool was tilted outwards in a given angle ϕ while the wall of the vase was tilting outwards, and vice versa. This was controlled by rotating the original rotation matrix relative to the global x- and y-axes shown in Fig. 13. The rotation matrices $\boldsymbol{R_x}$ and $\boldsymbol{R_y}$ are defined as [30]:

$$\boldsymbol{R_x} = \begin{bmatrix} 1 & 0 & 0 \\ 0 & \cos\alpha & -\sin\alpha \\ 0 & \sin\alpha & \cos\alpha \end{bmatrix} \tag{9}$$

and

$$\boldsymbol{R_y} = \begin{bmatrix} \cos\beta & 0 & \sin\beta \\ 0 & 1 & 0 \\ -\sin\beta & 0 & \cos\beta \end{bmatrix}. \tag{10}$$

The rotation angle ϕ for each layer can be read from table 2, and the rotations are given relative to the axes and points shown in Fig. 13. For the first part of the build, while the radius is increasing, the rotation angle ϕ is positive about the x- and y-axes for point p_2 and p_3, and negative for p_1 and p_4. For the last part of the build, while the radius is decreasing, the rotation angle ϕ is negative about the x- and y-axes for point p_2 and p_3, and positive for p_1 and p_4. The rotation matrix for the resulting rotation $\boldsymbol{R_N}$ at a given time is:

$$\boldsymbol{R_N} = \boldsymbol{R_0 R_{xR_y}}. \tag{11}$$

Table 2
Welding parameters for vase structure: Dynamic orientation of tool and predominantly using CMT welding.

Welding parameters for the vase structure shown in Fig. 12							
CMT, varying orientation of tool							
Method	Layer	Current(A)	Wire-feed sp.(m/min)	Voltage(V)	Radius(mm)	Bead height(mm)	Angle (ϕ)(degrees)
P-MIG	≈ **1**	182	7.1	25.5	60.0	1.22	20.0
P-MIG	≈ **2**	165	7.1	25.4	60.8	1.22	20.0
CMT	≈ **3–25**	108	4.0	15.4	61.6 + = 0.8	1.22	20.0
CMT	≈ **26–29**	95	3.8	15.9	80.0	1.46	20.0 -= 5.0
CMT	≈ **30–39**	95	3.8	15.9	80.0	1.70	0.0
CMT	≈ **40–44**	95	3.8	15.9	80 -= 0.64	1.54	0.0 -= 5.0
CMT	≈ **45–100**	95	3.8	15.9	76.8 -= 0.64	1.38	-25.0

The rotation is given relative to the axes in Fig. 13. The orientation only has to be defined for each of the four points p_1-p_4 in Fig. 13, as the linear RAPID functions `MoveC/ArcC` will distribute the change in orientation evenly over the arc between two points [29]. As the rotation angle ϕ at any of the four points will only be non-zero about either the x- or the y-axis, not both of them, the rotation matrix for the non-active axis will be equal to the identity matrix $\boldsymbol{I}$. In other words: Using equations 9-10, for each of the four points in Fig. 13 $\alpha = \phi$ and $\beta = 0$, or vice versa.

The quaternions $\boldsymbol{q_N}$ for this new orientation of the tool can then be found from the rotation matrix $\boldsymbol{R_N}$ using the approach presented in [32]. This approach avoids both dividing by zero and dividing by negative numbers. The rotation matrix $\boldsymbol{R_N}$ can be written as:

$$\boldsymbol{R_N} = \begin{bmatrix} r_{11} & r_{12} & r_{13} \\ r_{21} & r_{22} & r_{23} \\ r_{31} & r_{32} & r_{33} \end{bmatrix}. \tag{12}$$

Based on this, the following algorithm was used to find the quaternions [32]:

```
--------------------------------------------
%Finding quaternions from rotation matrix

T := R[1][1] + R[2][2] + R[3][3];
IF T > 0:
    S := Sqrt(1 + T)*2;
    qw := 0.25*S;
    qx := (R[3][2] - R[2][3])/S;
    qy := (R[1][3] - R[3][1])/S;
    qz := (R[2][1] - R[1][2])/S;
ELSEIF R[1][1]>R[2][2] AND R[1][1]>R[3][3]:
    S := Sqrt(1+R[1][1]-R[2][2]-R[3][3])*2;
    qw := (R[3][2] - R[2][3])/S;
    qx := 0.25*S;
    qy := (R[1][2] + R[2][1])/S;
    qz := (R[1][3] + R[3][1])/S;
ELSEIF R[2][2] > R[3][3]:
    S := Sqrt(1+R[2][2]-R[1][1]-R[3][3])*2;
    qw := (R[1][3] - R[3][1])/S;
    qx := (R[1][2] + R[2][1])/S;
    qy := 0.25*S;
    qz := (R[3][3] + R[3][2])/S;
ELSE:
    S := Sqrt(1+R[3][3]-R[1][1]-R[2][2])*2;
    qw := (R[2][1] - R[1][2])/S;
    qx := (R[1][3] + R[3][1])/S;
    qy := (R[2][3] + R[3][2])/S;
    qz := 0.25*S;
ENDIF
--------------------------------------------
```

?.

This method follows what is described in chapter 6 of [30], based on [33]. First, the trace of the rotation matrix $\boldsymbol{R_N}$ is found, i.e. the sum of the diagonal terms:

$$T = r_{11} + r_{22} + r_{33} = r_{00}. \tag{13}$$

If defining $\boldsymbol{z} = 2\boldsymbol{q}$, this gives us the set of equations [30]:

$$z_0^2 = 1 + 2r_{00} - T \tag{14}$$

$$z_1^2 = 1 + 2r_{11} - T \tag{15}$$

$$z_2^2 = 1 + 2r_{22} - T \tag{16}$$

$$z_3^2 = 1 + 2r_{33} - T, \tag{17}$$

and

$$z_0 z_1 = r_{32} - r_{23} z_2 z_3 = r_{32} + r_{23} \tag{18}$$

$$z_0 z_2 = r_{13} - r_{31} z_3 z_1 = r_{13} + r_{31} \tag{19}$$

$$z_0 z_3 = r_{21} - r_{12} z_1 z_2 = r_{21} + r_{12}. \tag{20}$$

Using the ten expressions from equations 14-20, the four unknowns z_0-z_3 can be found using many different approaches, as the variables r_{00-33} are known [33]. The quaternions $\boldsymbol{q_N}$ describing the new rotation can then be found, as

$$\boldsymbol{z} = 2\boldsymbol{q_N}. \tag{21}$$

The radius of each approx. layer of the vase, which determines how much each layer shifted relative to the previous layer, are listed in table 2. This shift, and the angle of the tilt of the wall of the vase, impacted on how much the deposited material would spread out before cooling down and solidifying, as explored in [34]. This implies that the estimated layer height became lower the steeper the building angle. This was accounted for during the build by setting the layer height to be a function of the change in angle, and the different layer heights are listed in Table 2. The correlation between layer height, tilt angle and change in radius, was linear, and set based on trial and error until finding a tilt angle for the welding gun that followed the tilt of the wall to some extent, though not accurately. A large angle would give a significant reduction in layer height and a large change in radius. The values used for the height increase, and how the angle of the tool was adjusted relative to the inclination of the wall, is based on experience from the experiments presented in *Continuous build of thin-walled structures–Fixed orientation of tool: Twisting hexagon*.

The build continued for approx. 100 layers, and was stopped because the welding material ran out. The final layer was shifted several centimetres relative to the vertical part of the structure, which shows that it was possible to build a significant overhang using non-vertical material deposition.

Table 3
Welding parameters for bowl structure: Dynamic orientation of tool and predominantly using CMT welding.

Welding parameters for bowl structure shown in Fig. 15							
CMT, varying orientation of tool							
Method	Layer	Current(A)	Wire-feed sp.(m/min)	Voltage(V)	Radius(mm)	Bead height(mm)	Angle (ϕ)(degrees)
P-MIG	≈ **1**	180	7.1	25.9	40.0	1.30	0.0
P-MIG	≈ **2**	156	7.1	25.2	40.0	1.30	0.0
CMT	≈ **3**	140	6.6	18.8	40.0	1.30	0.0
CMT	≈ **4**	108	3.9	15.8	40.0	1.30	0.0
CMT	≈ **5**	108	3.9	15.8	40.0	1.30	0.0
CMT	≈ **6–48**	96	3.5	14.0	40.0 + = 1.30·sin ϕ	1.30·cos ϕ	1.0 + = 1.0
CMT	≈ **49–96**	96	3.5	14.0	55.7 + = 0.89	0.95	43.0

Non-vertical material deposition: Bowl

After the build described in *Non-vertical material deposition: Vase*, a structure with a more significant overhang was constructed using non-vertical material deposition. Another variation of the cylinder structures presented in *Continuous build of thin-walled structures* and *Set-based control for flexibility in orientation of tool* was chosen, the alteration this time being a constantly increasing radius. This would result in a kind of bowl, in parts similar to the bottom part of the vase structure in Fig. 12, described in *Non-vertical material deposition: Vase*. The aim was to see how successful a continuous build of a structure with an increasing overhang would be, and if a overhang of more than 25° would prove challenging considering the material deposition when building in a similar material. The build was done using the nickel alloy Inconel 625, which is the same material used to build the flower structure shown in Fig. 6b. The substrate was made of carbon steel S355G10.

As in earlier builds, the increase in height of the welding gun accounting for each added layer was distributed over the last quadrant of each circular layer, thereby avoiding the issues that came with a height increase in a single point shown in Fig. 4. The initial layer height was slightly lowered compared to the vase build: from 1.7 mm to 1.3 mm in the part where the welding gun had a strictly vertical orientation. The radius and layer height was kept constant for the first 5 layers of the build, and the orientation of the tool was kept strictly vertical. This to get a good foundation for the rest of the build. As with all previous builds, the first few layers demanded a higher heat input than the rest of the build in order for the material to adhere properly to the substrate. The first two layers of the bowl structure were welded using pulsed MIG, as with the vase structure. The welding procedure was then paused momentarily to switch to CMT welding. The welding parameters for the complete build were based on parameters of the vase build in *Non-vertical material deposition: Vase*, and are described in detail in Table 3.

After the 5 first layers, the orientation of the tool was adjusted to increase by 1° per layer. The orientation of the welding gun was controlled as described in *Non-vertical material deposition: Vase*, always tilting inwards as shown in Fig. 12a. As explained in *Non-vertical material deposition: Vase*, the symmetry of the nozzle meant that the rotations only had to be performed relative to the global x- and y-axis. Because the angle would only increase relative to a vertical position, the bowl build was similar to the bottom-most part of the vase build, only with an increasing rather than decreasing overhang. While the angle increased, the radius would also increase slightly, creating a wall with a stronger tilt. As these changes were made in parallel, the angle of the welding gun would follow the building direction of the wall.

The larger the angle of the welding gun became, the more the radius would increase per layer. This made sense considering that a larger angle meant that the gravity to a larger extent could pull on the deposited, melted material so that it would spread out more before becoming solid. As the liquid material would spread out more horizontally, the layer height would simultaneously decrease. For the vase structure, these values were adjusted in a similar fashion, but there was no exact correlation between the angle of the welding gun and the tilt of the wall: the values were set more based on trial-and-error. For the bowl structure, the angle ϕ was increased by 1° per layer, and the initial layer height was set to 1.3 mm, based on the results from the vase structure. For this experiment, we wished to see how the build would progress when the increase in radius r_{inc} and the current layer height l_{hc} were set according to the geometrical correlation between these values as seen in a right triangle shown in Fig. 14. Following basic trigonometry, the layer height was set as

$$l_{hc} = l_h \cdot \sin\phi, \tag{22}$$

and the increase in radius for each layer was set as

$$r_{inc} = l_h \cdot \cos\phi. \tag{23}$$

For the first layers, while the angle ϕ was kept at zero, the increase in radius was also equal to zero, and the layer height was fixed at the set value 1.3 mm. Then, as the angle ϕ increased by 1° per layer, the radius would increase and the layer height would decrease. Using the simulation software Robot Studio from ABB, the designed path for this structure was simulated, as shown in Fig. 15a. During these simulations, the 6 DOF robot manipulator would face issues with singularities or joints being out of bounds when the angle ϕ got close to 50°, depending on the start position of the tool. To avoid this issue when performing the build, a maximum angle ϕ_{max} was set to 43°. As the aim of this build was to build a structure with a significantly larger overhang than that of the 20–25° overhang of the vase presented in *Non-vertical material deposition: Vase*, this was considered sufficient. When reaching this maximum angle ϕ_{max}, the build would continue on with this angle until stopped, resulting in the structure shown in Fig. 12c and d. For this final part of the build, the layer height would stay fixed at a value given by Eq. 22, and there would be an increase in the radius r_{inc} per additional layer given by Eq. 23, both with $\phi = \phi_{max}$.

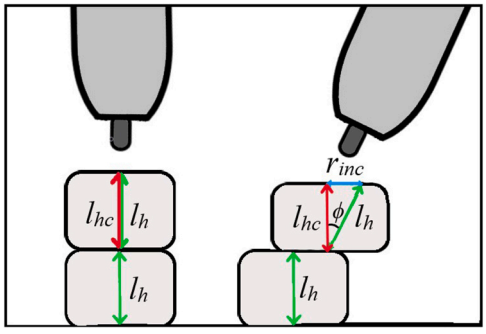

Fig. 14. Angle variation: As shown here, the layer height has a fixed value while the welding gun is strictly vertical. As the angle ϕ grows, this initial layer height becomes the hypotenuse in a right triangle. The layer height l_{hc} for the new layer, displayed in red, is described by equation 22. The increase in radius r_{inc}, displayed in blue, is described by equation 23.

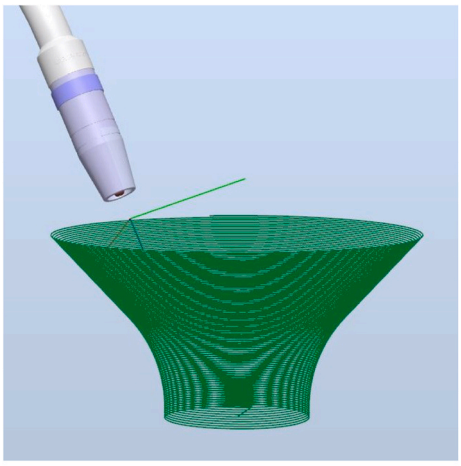

(a) The simulated path for the structure with 43° overhang.

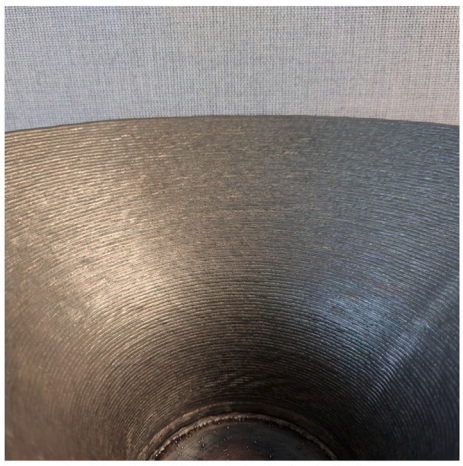

(b) The build was smooth, without clear deformations

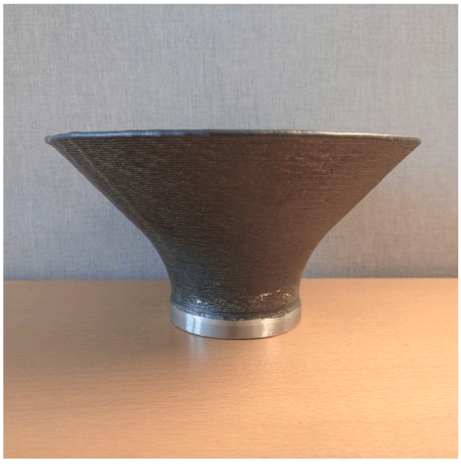

(c) The final 43° overhang of the bowl.

(d) The final bowl.

Fig. 15. The structure had a gradually increasing overhang, moving from a tilt of 0° to 43°, relative to a vertical orientation of the welding gun.

Material analysis

The conditions for heat accumulation and heat dissipation are altered when building with overhangs and intersections. As a consequence, the cooling rate and thermal gradient during solidification of the material is different along the trajectory. The different thermal history may lead to promotion of other phases and microstructures, which in turn may influence the mechanical properties and service performance. To better understand the effect of non-steady state deposition, the hexagonal structure in Fig. 11 and the flower shape in Fig. 7 were examined. Transverse sections of stable mid-wall positions, overhang corners, and intersection were examined by optical microscopy and hardness measurements to reveal any process defects or fluctuations. Both materials were manufactured with the Ni-Cr-Mo alloy UTP 759.

The hexagonal structure is shown in Fig. 16. The mid-wall position, i.e., with no overhang shows a mixed structure of columnar and equiaxed dendrites. The dendrites were nearly vertically oriented, i.e. parallel to the building direction. This structure was developed due to the strong heat sink of the already built structure by thermal conduction. The columnar dendrites grew over several layers, due to epitaxial nucleation upon remelting and solidification of a new layer. Columnar dendrites ranging over several layers are commonly seen in WAAM of nickel-based alloys like Hastelloy C276 and Inconel 625 [35–37]. A portion of equiaxed 'star-shaped' dendrites can also be seen in Fig. 16a. This morphology is uncommon in lean alloys like Hastelloy C276 and Inconel 625 processed by WAAM. However, UTP 759 has a higher alloying content, so the constitutional undercooled zone was larger during solidification compared to Hastelloy C276 and Inconel 625. This effect increased the probability of nucleation ahead of the columnar growth front and created the equiaxed dendrites.

The microstructure at the overhang position is shown in Fig. 16b. The structure was solely occupied by fine equiaxed dendrites. As the chemical composition is similar irrespective of position, the altered thermal characteristics are responsible for this microstructural change compared to the mid-wall position with no overhang. When the material is deposited with overhangs, a lower portion of the liquid weld bead is in direct contact with the former layer. Consequently, the downward thermal gradient due to conduction is decreased compared to a structure with no overhang. With a lower thermal gradient, the driving force for columnar growth is decreased and the constitutional undercooling increases. Such conditions are facilitating the nucleation of equiaxed dendrites. Overhangs can therefore influence the microstructure and the related properties of WAAM structures. Small process defects were occasionally observed at the bead interface when building with overhangs, such as the black lack-of-fusion defects depicted in Fig. 16b. Further process parameter optimisation is required to eliminate such defects.

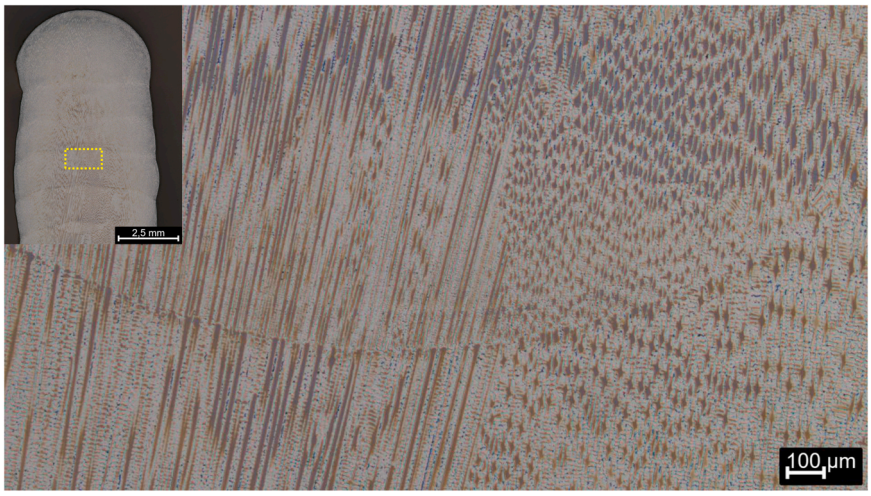

(a) Hexagon mid-wall position with no overhang. Mixture of columnar and equiaxed dendrites.

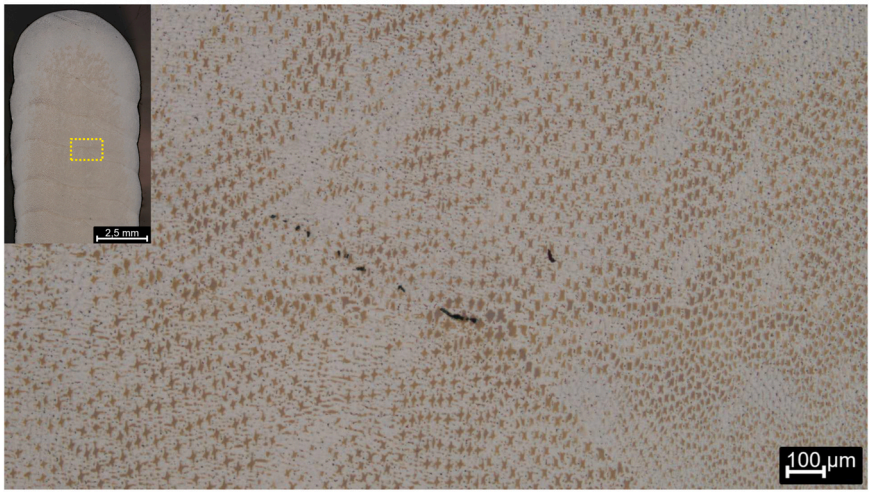

(b) Hexagon corner position with overhang. Structure with fine equiaxed dendrites.

Fig. 16. Microstructure of Ni-Co-Mo alloy UTP 759 hexagon structure in transverse section.

The microstructure of the flower shaped structure is shown in Fig. 17. This design has no overhangs, but two touching corners to create a continuous intersection. The intersection involves an extra remelting step of the structure, and two bead junctions can be observed in Fig. 17b. This effect has a minor influence on the final microstructure. The material exhibits a relatively homogeneous structure of equi-axed dendrites regardless of position. The only exception to this statement is some scattered columnar dendrites in vicinity of remelted layers at intersections, Fig. 17b. There was not observed any process defects as cracks, pores or lack of fusion in the structure.

It is evident that the microstructure during 'normal' deposition (i.e., no overhang or intersections) is different for the hexagonal structure and the flower structure. This difference is related to the increased heat input when under deposition of the flower shape. A higher heat input was necessary to ensure fusion at the intersection zone of the flower. The increased heat input lowers the temperature gradient in the molten weld pool, which in turn suppress the columnar dendritic growth. The effect of heat input and microstructure was evaluated by Vickers hardness testing, see Fig. 18. The hexagon geometry with no overhang possessed a mixture of columnar and equiaxed dendrites. The anisotropic properties of the columnar structure resulted in lower hardness values, and increased the result scatter. Further, the flower shape showed similar to somewhat higher hardness compared to the hexagon structure. Refined equiaxed dendrites accounted for the observed increase in hardness. In-depth assessments of mechanical performance, e.g. tensile strength, impact toughness, fatigue- and creep resistance was out of scope of this work, but should be assessed in further work.

Discussion

The experiments presented in this paper all take a step away from in-box, strictly layer-based AM methods. For the preliminary experiments, the trajectory for the walls resembles an upwards spiralling helix. This differs from the strictly layer-by-layer approach that you find in AM methods such as VP or PBF. After the preliminary experiments using a form of viscous glue, the focus of this research turned to metals and the DED method WAAM. Performing the builds as continuously as possible was still a priority, as the initiation or termination of the material deposition often brings with it some deformations and inaccuracies in the material deposition. In *Continuous build of thin-walled structures* it is also examined how, when deposition material continuously, a gradual transition between layers can give fewer distortions for WAAM than an height increase in a single point, as is common for many AM methods.

WAAM using CMT and pulsed-MIG gave results with few distortions when building thin-walled structures. For simple

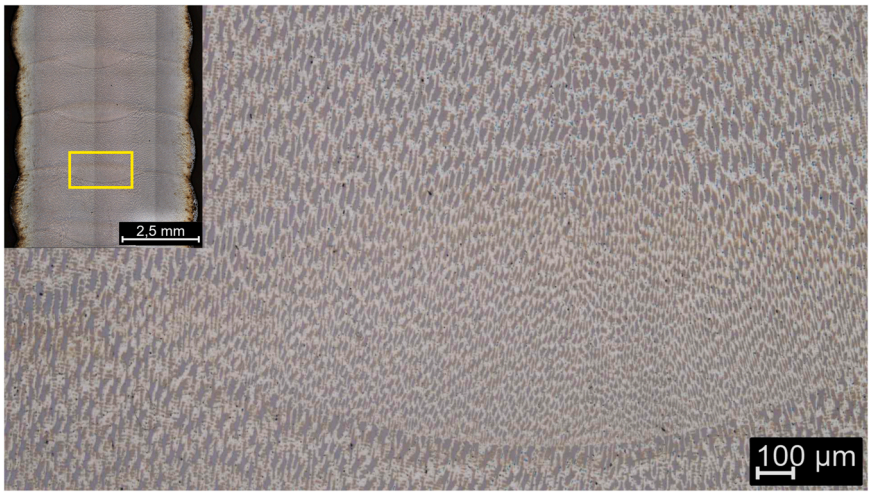

(a) Flower mid-wall position. Structure with fine equiaxed dendrites.

(b) Flower intersection. Mixture of columnar and equiaxed dendrites.

Fig. 17. Microstructure of Ni-Co-Mo alloy UTP 759 flower structure in transverse section.

geometrical structures such as a cylinder, both metals with a low and a high melting point resulted in structures with few deformations. These builds could have continued for a long time due to an equilibrium between heat accumulation and dissipation. For slightly more complex structures with intersections, described in *Avoiding double material deposition in intersections*, it proved easier to get a result with few deformations when using metals with a higher melting point. This is to be expected: The lower the melting point, the higher the risk of the accumulated heat impacting how long the deposited material takes to solidify, resulting in an uneven distribution of the deposited material. To cross-check the results from the experiments presented here, additional structures based on the principle described in *Continuous build of thin-walled structures* and 5 were built using the Ni-Cr-Mo alloy UTP 759. As can be seen by comparing Fig. 19 with Fig. 5 and 7, a harder material with a higher melting point helped make the surface of the structures smoother and with less superficial deformations compared to similar structures built in aluminium alloys.

The hexagonal structure presented in *Fixed orientation of tool: Twisting hexagon* shows that if the material solidifies quickly enough, it is possible to build overhangs even when depositing material from a nozzle with a vertical orientation. Future work should look into how the same structure will turn out when building in a softer material with a lower melting point, such as the aluminium-alloys used in other builds described in this paper. It would also be interesting to examine how a structure in the same material would behave with a larger rotation angle, which would lead to less overlap between two consecutive layers. The optical microscopy and hardness

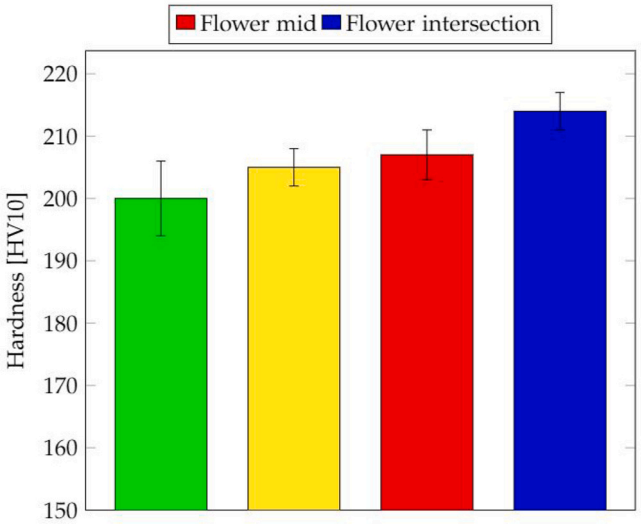

Fig. 18. Vickers hardness of Ni-Cr-Mo alloy UTP 759.

Fig. 19. Additional structures were constructed in the Ni-Cr-Mo alloy UTP 759.

measurements presented in *Material analysis* showed that such an approach will influence the micro structure of the component, but it did not seem to have significant impact on the hardness, as shown in Fig. 18.

The set-based approach used in [17] could be used for the simple thin-walled structure without overhang described in *Set-based control for flexibility in orientation of tool*. The additional freedom in orientation of the tool given by the set-based control method could potentially save energy while performing the build in the same amount of time, as shown in [20]. The method also required less torques in the turns, as the tool did not have to keep one strict orientation, which made it possible to perform sharp turns and sharp changes in the direction of the path faster and smoother. This was useful, as the earliest welding tests with the box-shape described in *Continuous build of thin-walled structures* showed that if the corners were too sharp, material would accumulate because the welding gun stayed in the same spot too long while the robot re-configured itself for the change in direction [16]. However, this structure did show some prominent deformations compared with similar structures in Fig. 5 and 19. The saddle form at the top of the finished structure was likely caused by the non-symmetric deviation in the orientation of the welding gun. This unpredictable imprecision can make the method unsuitable depending on the specifications for the built structure.

When building the vase-structure with very prominent overhangs it quickly became evident that when building a significant overhang with less vertical alignment between two consecutive layers, the orientation of the tool needed to be controlled much more closely. The freedom given by the set-based control method did not distribute the change in the orientation of the tool symmetrically, which made the method unsuited for the task. The experiment described in the first part of *Non-vertical material deposition: Vase* showed that the results could be quite unpredictable. A vertical orientation of the tool while deposition material on a wall that tilted gave a poor result, as the overlap with the previous layer was not large enough.

When constructing a vase shape with the nozzle of the welding gun following the tilt of the wall of the structure, the results were more promising. The angle of the tilt for the first part of the build showed that the build could be affected as the heat built up early in the build. In Fig. 12 it is possible to see that even though the angle of the bottom part of the vase was constant for this part of the build, the tilt of the wall seemed to decrease slightly after a few centimetres. This was caused by the accumulated heat in the structure: As the structure heated up, it took slightly longer for the deposited material to solidify, making the welding bead flatter and wider. As the angle of the top part of the vase, above the vertical part of the wall, did not have any such irregularities, it can be concluded that at this point the accumulated heat and the heat dissipation had reached equilibrium, making the welded wall smoother. The bowl structure presented in *Non-vertical material deposition: Bowl* did not have this same slope in angle. This might be because the first few layers were built straight up, with a vertical orientation of the welding gun. By the time the overhang became prominent enough for such drooping to take place, the heat dissipation had already reached equilibrium, so that the build was smooth from thereon.

The distance between the tool and surface to be welded grew too large during the vase build. If the distance between the nozzle and the surface grows too large, this can make the arc unstable and lead to deformations, as well as reduce the protective effects of the shielding gas [38]. An inaccurate estimate of the layer height was also an issue in earlier builds, most-times solved by interrupting the build to adjust the distance between the nozzle and the structure [16]. Based on the results from the vase build, the initial layer height was reduced for the bowl build, from 1.7 mm to 1.3 mm when the welding tool was vertical. In addition, the layer height for the build was set as a trigonometrical function of the angle of the welding gun relative to a vertical orientation. This seemed to be a good proximate for how the bead height and width developed as the build went on. Unlike for the vase build, the distance between the tool and the surface did not grow too large during the bowl build, and the build could have continued for longer if desired.

For future experiments, layer heights throughout the build relative to the angle of the tilt of an overhang should be adjusted more accurately. For the vase structure in *Non-vertical material deposition: Vase*, all values were estimated based on the experience from the experiments presented in Continuous build of thin-walled structures [16] and *Set-based control for flexibility in orientation of tool* [17]. More accurate estimates could be made, for example based on the results from [34] or [39]. If these values were optimised, it might be possible to build similar overhangs in other metals with a lower melting point, such as aluminium. The issue could also be solved either by adjusting the vertical position of the nozzle during the build, or by ensuring a more stable layer height [38].

Building structures with even larger overhangs can also be considered future work. As explained in *Non-vertical material deposition: Bowl*, the 6 DOF robot manipulator met challenges such as joint out of bounds or singularities when the angle of the bowl grew larger than the set maximum angle of 43°. Avoiding these issues would perhaps require an alternative control method altogether than that of the built-in functions of the RAPID programming language. At least it would have required more time adjusting the set-up of the robot cell, and the start point and orientation of the end effector. Building a basic, tilted wall would have been possible without the robot reaching singularities. Such thin-walls have been investigated by others, for example in [39]. As the main goal was to show that the construction of a prominent overhang with continuous, non-vertical material deposition was possible, a 43° angle was considered sufficient, and further adjustments are considered out of scope for the work presented here.

Concluding remarks

Building using WAAM is a relatively easily accessible way to enable non-vertical-deposition of material, as welding equipment combined with an industrial robot manipulator can be found in many labs and factories. Other projects have gotten very interesting results using other materials than metals and WAAM, such as fast-curing polymers [12]. This should be explored in future work.

Throughout the welding experiments presented in this paper, the distance between the nozzle of the welding gun and the surface to be welded was adjusted manually by the welding operator during several of these builds. A more solid solution could be to include

feedback in the process. The welding parameters, i.e. current and voltage, are impacted by this distance. If these values were monitored during the build, it could be possible to detect if this distance grew too large or too small, and the controller could then modify the path accordingly. Ideally, these adjustments could also be included in a feed-back loop and done automatically, enabling the process do correct itself during the build. This kind of feedback could potentially also be used to find an optimal orientation of the tool relative to the overhang, as the size of the contact surface is largest when the tool is orthogonal to the direction of the construction [39]. This should explored in future work.

The set-based control method designed by Moe et al. [19] was not well suited for building structures with overhangs, as the deviation in orientation was unpredictable an non-symmetrical. The method might work better if it was possible to restrict the set of valid angles for the tool further, but this would somewhat contradict the main benefits of the control method. In future work, it could be examined if this method can be modified to distribute the orientation evenly about a fixed point.

Several of the experiments showed that it is important to adjust the heat-input so that the structure does not grown too hot due to accumulated heat. This could be seen very clearly on the final vase-shape, where accumulated heat due to a large heat input early in the build made the walls of the structure slope more than estimated. Controlling that the heat input and heat dissipation is as close as possible to an equilibrium can for example be done by monitoring the accumulated heat in the structure during the build. The bowl build with an overhang of 43° shows that it is possible to construct thin-walled structures with prominent overhangs using continuous, non-vertical material deposition. Future work should examine how steep and large such an overhang could be before the structure showing significant deformations, preferably for different materials. A more thorough material analysis of structures with overhangs, including in-depth assessment of the tensile strength, impact toughness, fatigue- and creep resistance should also be examined in future work, but was out of scope for this work.

Funding

The work reported in this paper was based on activities within centre for research based innovation SFI Manufacturing in Norway, and is partially funded by the Research Council of Norway under contract number 237900.

Declaration of Competing Interest

The authors declare that they have no known competing financial interests or personal relationships that could have appeared to influence the work reported in this paper.

References

[1] Gibson, I., Rosen, D.W., Stucker, B., 2010, Additive Manufacturing Technologies, 238. Springer.
[2] Abdulhameed, O., Al-Ahmari, A., Ameen, W., Mian, S.H., 2019, Additive Manufacturing: Challenges, Trends, and Applications. Advances in Mechanical Engineering, 11/2:1687814018822880https://doi.org/10.1177/1687814018822880.
[3] Oliveira, J., LaLonde, A., Ma, J., 2020, Processing Parameters in Laser Powder Bed Fusion Metal Additive Manufacturing. Materials & Design, 193:108762https://doi.org/10.1016/j.matdes.2020.108762.
[4] Apis-cor.com, Apis-cor, accessed 2021–11-04 (2015–2021).⟨https://www.apis-cor.com⟩.
[5] Kampc.be, 3d-printing in the construction world, accessed 2021–11-04 (2018–2021).⟨https://www.kampc.be/c3po_eng⟩.
[6] Jiang, J., Ma, Y., 2020, Path Planning Strategies to Optimize Accuracy, Quality, Build Time and Material Use in Additive Manufacturing: A Review. Micromachines, 11/7: 633. https://doi.org/10.3390/mi11070633.
[7] Jiang, J., Xu, X., Stringer, J., 2018, Support Structures For Additive Manufacturing: A Review. Journal of Manufacturing and Materials Processing, 2/4: 64. https://doi.org/10.3390/jmmp2040064.
[8] Dai, C., Wang, C.C., Wu, C., Lefebvre, S., Fang, G., Liu, Y.-J., 2018, Support-free Volume Printing by Multi-axis Motion. ACM Transactions on Graphics ((TOG)), 37/4: 134. https://doi.org/10.1145/3197517.3201342.
[9] Panchagnula, J.S., Simhambhatla, S., 2018, Manufacture of Complex Thin-walled Metallic Objects Using Weld-deposition Based Additive Manufacturing. Robotics and Computer-Integrated Manufacturing, 49:194–203. https://doi.org/10.1016/j.rcim.2017.06.003.
[10] Parmar, K., Oster, L., Mann, S., Sharma, R., Reisgen, U., Schmitz, M., Nowicki, T., Wiartalla, J., Hüsing, M., Corves, B., 2021, Development of a Multidirectional Wire Arc Additive Manufacturing (waam) Process with Pure Object Manipulation: Process Introduction and First Prototypes. Journal of Manufacturing and Materials Processing, 5/4: 134. https://doi.org/10.3390/jmmp5040134.
[11] Jorislaarman.com, MX3D bridge, accessed 2019–11-11 (2015–2019).⟨https://www.jorislaarman.com/work/mx3d-bridge/⟩.
[12] Laarman, J., Jokic, S., Novikov, P., Fraguada, L.E., Markopoulou, A., 2014, Anti-gravity Additive Manufacturing. Fabricate: Negotiating Design & Making, 192–197. https://doi.org/10.2307/j.ctt1tp3c5w.27.
[13] Ramalho, A., Santos, T.G., Bevans, B., Smoqi, Z., Rao, P., Oliveira, J., 2022, Effect of Contaminations on the Acoustic Emissions During Wire and Arc Additive Manufacturing of 316l Stainless Steel. Additive Manufacturing, 51:102585https://doi.org/10.1016/j.addma.2021.102585.
[14] Ding, D., Pan, Z., Cuiuri, D., Li, H., 2015, A Practical Path Planning Methodology for Wire and Arc Additive Manufacturing of Thin-walled Structures. Robotics and Computer-Integrated Manufacturing, 34:8–19. https://doi.org/10.1016/j.rcim.2015.01.003.
[15] Evjemo, L.D., Moe, S., Gravdahl, J.T., Roulet-Dubonnet, O., Gellein, L.T., Brøtan, V., 2017, Additive Manufacturing by Robot Manipulator: An Overview of the State-of-the-art and Proof-of-concept Results. 22nd IEEE ETFA, Cyprus: 1–8. https://doi.org/10.1109/ETFA.2017.8247617.
[16] Evjemo, L.D., Langelandsvik, G., Gravdahl, J.T., 2019, Wire Arc Additive Manufacturing by Robot Manipulator: Towards Creating Complex Geometries. 5th IFAC ICONS. Elsevier, Belfast: 103–109. https://doi.org/10.1016/j.ifacol.2019.09.125.
[17] Evjemo, L.D., Moe, S., Gravdahl, J.T., 2020, Robotised Wire Arc Additive Manufacturing Using Set-based Control: Experimental Results. 21st IFAC World Congress, Berlin: 1–8. https://doi.org/10.1016/j.ifacol.2020.12.2725.
[18] Würth, SikkerhetsdatabladSTP Quickfast hvit 290 ml, rev. 3.1, ⟨https://www.wuerth.no/msds/pdf/01275205.PDF⟩ (2)2016.
[19] Moe, S., Antonelli, G., Teel, A.R., Pettersen, K.Y., Schrimpf, J., 2016, Set-Based Tasks within the Singularity-Robust Multiple Task-Priority Inverse Kinematics Framework: General Formulation, Stability Analysis, and Experimental Results. Frontiers in Robotics and AI, 3/April: 1–18. https://doi.org/10.3389/frobt.2016.00016⟨http://journal.frontiersin.org/article/10.3389/frobt.2016.00016⟩.
[20] Moe, S., Gravdahl, J.T., Pettersen, K.Y., 2018, Set-based Control for Autonomous Spray Painting. IEEE Transactions on Automation Science and Engineering, 15/4: 1785–1796. https://doi.org/10.1109/TASE.2018.2801382.
[21] Halmøy, E., 1991, Sveiseteknikk. 4th edition NTNU, Norway.
[22] Cong, B., Ouyang, R., Qi, B., Ding, J., 2016, Influence of Cold Metal Transfer Process and its Heat Input on Weld Bead Geometry and Porosity of Aluminum-copper Alloy Welds. Rare Metal Materials and Engineering, 45/3: 606–611. https://doi.org/10.1016/S1875-5372(16)30080-7.
[23] Abb.com, IRB 2400, accessed 2018–10-22 (2016–2018).⟨https://new.abb.com/products/robotics/industrial-robots/irb-2400⟩.
[24] Fronius.com, CMT - cold metal transfer: The cold welding process for premium quality, accessed 2021–07-28 (2019–2021).⟨https://www.fronius.com/en/welding-technology/world-of-welding/fronius-welding-processes/cmt⟩.
[25] Smati, Z., 1986, Automatic Pulsed Mig Welding. .
[26] Martina, F., Mehnen, J., Williams, S.W., Colegrove, P., Wang, F., 2012. Investigation of the benefits of plasma deposition for the additive layer manufacture of Ti-6Al-4V, 212 (6),1377–1386, 10.1016/j.jmatprotec.2012.02.002.
[27] Mehnen, J., Ding, J., Lockett, H., Kazanas, P., 2011, Design for Wire and Arc Additive Layer Manufacture. Global Product Development Springer: 721–727. https://doi.org/10.1007/978-3-642-15973-2_73.
[28] Cade, P., Gordon, R.A., 2005, An Apothem Apparently Appears. The College Mathematics Journal, 36/1: 52–55. https://doi.org/10.2307/30044819.
[29] ABBRobotics, Technical reference manual: RAPID Instructions, Functions and Data types (2004–2010).
[30] Egeland, O., Gravdahl, J.T., 2002, Modeling and Simulation for Automatic Control. Marine Cybernetics Trondheim, Norway.
[31] Kuipers, J.B., 1999, Quaternions and Rotation Sequences: A Primer with Applications to Orbits, Aerospace, and Virtual Reality. Princeton University Press.
[32] Euclidianspace.com, Maths - conversion matrix to quaternions, accessed 2021–04-03 (1999–2007).⟨https://www.euclideanspace.com/maths/geometry/rotations/conversions/matrixToQuaternion/⟩.

[33] Shepperd, S.W., 1978, Quaternion From Rotation Matrix. Journal of Guidance and Control, 1/3: 223–224. https://doi.org/10.2514/3.55767b.
[34] Jiang, J., Stringer, J., Xu, X., Zhong, R.Y., 2018, Investigation of Printable Threshold Overhang Angle in Extrusion-based Additive Manufacturing for Reducing Support Waste. International Journal of Computer Integrated Manufacturing, 31/10: 961–969. https://doi.org/10.1080/0951192X.2018.1466398.
[35] Qiu, Z., Wu, B., Zhu, H., Wang, Z., Hellier, A., Ma, Y., Li, H., Muransky, O., Wexler, D., 2020, Microstructure and Mechanical Properties of Wire Arc Additively Manufactured Hastelloy C276 Alloy. Materials & Design, 195:109007https://doi.org/10.1016/j.matdes.2020.109007.
[36] Qiu, Z., Wu, B., Wang, Z., Wexler, D., Carpenter, K., Zhu, H., Muránsky, O., Zhang, J., Li, H., 2021, Effects of Post Heat Treatment on the Microstructure and Mechanical Properties of Wire Arc Additively Manufactured Hastelloy C276 Alloy. Materials Characterization, 177:111158https://doi.org/10.1016/j.matchar.2021.111158.
[37] Yangfan, W., Xizhang, C., Chuanchu, S., 2019, Microstructure and Mechanical Properties of Inconel 625 Fabricated by Wire-arc Additive Manufacturing. Surface and Coatings Technology, 374:116–123. https://doi.org/10.1016/j.surfcoat.2019.05.079.
[38] Shen, H., Deng, R., Liu, B., Tang, S., Li, S., 2020, Study of the Mechanism of a Stable Deposited Height During Gmaw-based Additive Manufacturing. Applied Sciences, 10/12: 4322. https://doi.org/10.3390/app10124322.
[39] Xiong, J., Lei, Y., Chen, H., Zhang, G., 2017, Fabrication of Inclined Thin-walled Parts in Multi-layer Single-pass Gmaw-based Additive Manufacturing with Flat Position Deposition. Journal of Materials Processing Technology, 240:397–403. https://doi.org/10.1016/j.jmatprotec.2016.10.019.